Live-cell chromosome dynamics in *Arabidopsis thaliana* reveals increased chromatin mobility in response to DNA damage

Anis Meschichi[1], Svenja Reeck[2], Adrien Sicard[1], Frédéric Pontvianne[3], Stefanie Rosa[1#]

[1] *Swedish University of Agricultural Sciences, Plant Biology Department, Uppsala, Sweden.*
[2] John Innes Centre, Norwich Research Park, Norwich NR4 7UH, United Kingdom
[3] *CNRS, Laboratoire Génome et Développement des Plantes (LGDP), Université de Perpignan Via Domitia, Perpignan, France*
[#] corresponding author: Stefanie.rosa@slu.se

SUMMARY

Double-strand breaks (DSBs) are a particularly deleterious type of DNA damage potentially leading to translocations and genome instability. Homologous recombination (HR) is a conservative repair pathway in which intact homologous sequences are used as a template for repair. How damaged DNA molecules search for homologous sequences in the crowded space of the cell nucleus is, however, still poorly understood. Here, we measured global chromosome and DSB site mobility, in *Arabidopsis thaliana,* using *lacO*/LacI tagged lines and two GFP-tagged HR regulators, RAD51 and RAD54. We observed an increase in chromatin mobility upon the induction of DNA damage, specifically at the S/G2 phases of the cell cycle. Importantly, this increase in mobility was lost in *sog1-1* mutant, a central transcription factor of the DNA damage response (DDR), indicating that repair mechanisms actively regulate chromatin mobility upon DNA damage. Interestingly, we observed that DSB sites show remarkably high mobility levels at the early HR stage. Subsequently, a drastic decrease of DSB mobility is observed, which seems to be associated to the relocation of DSBs to the nucleus periphery. Altogether, our data suggest that changes in chromatin mobility are triggered in response to DNA damage, and that this may act as a mechanism to enhance the physical search within the nuclear space to locate a homologous template during homology-directed DNA repair.

RESULTS AND DISCUSSION

Among the different types of DNA damage, double-strand breaks (DSBs) are particularly harmful for cells[1]. Therefore, efficient and accurate repair mechanisms are essential to maintain genome integrity, especially in sedentary organisms with late germline differentiation, such as plants. In plants, the DDR master regulator SUPPRESSOR OF GAMMA RESPONSE 1 (SOG1) initiates a repair response by inducing the transcription of genes involved in cell cycle arrest and repair[2–4]. Among DDR responsive genes there are several genes directly linked to the HR pathway[5,6]. Central to this pathway is the homology search and the DNA strand invasion reaction, which requires a homologous DNA template. The molecular processes that control HR have been extensively characterized (see [7,8] for review). However, the mechanisms behind the search and recognition of homologous sequences is still not well understood. To measure chromatin mobility in living cells we used the *lacO*/LacI-GFP locus-tagging system [9,10] (Fig. 1A) and quantified foci mobility using a mean square displacement (MSD) analysis. This analysis robustly measures the mobility of diffusing, fluorescently tagged chromosomal loci and provides kinetic parameters describing loci motion[11,12]. We first tested our setup by measuring “steady-state” chromatin mobility levels for cells in the division versus differentiation zones of the Arabidopsis root (Fig. 1B). Measurements of histone exchange dynamics had previously shown that cells at the division zone have a more dynamic chromatin state as compared to differentiated cells[13,14]. Consistently, we observed that chromatin mobility is also higher in cells from the division zone compared to cells from the differentiation zone (Fig. 1C). Accordingly, the radius of constrain (Rc), which indicates the nuclear volume within which a fluorescent spot can move, was significantly higher in

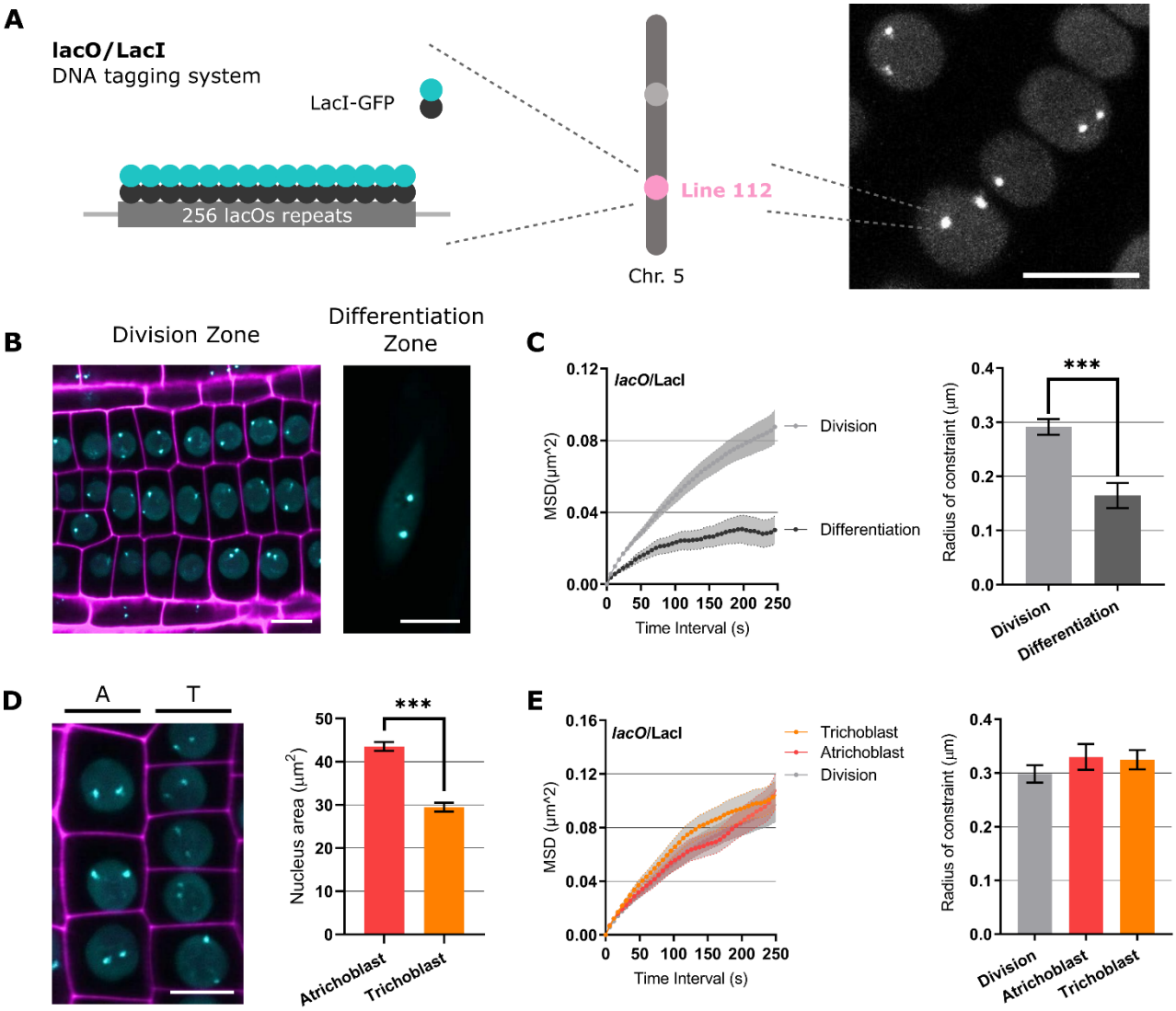

Figure 1: MSD analysis of *lacO* foci in different cell types in *Arabidopsis thaliana* root. (**a**) Schematic representation of the *lacO*/LacI system. A *lacO* repeat array was integrated into chromosome 5 (line112) and detected by expression of the LacI protein fused to GFP. The image on the right corresponds to z-projected images from root epidermal nuclei expressing the referred construct. Scale bar, 10µm (**b**) Representative images of the Arabidopsis root epidermal cells in division (left image) and differentiation zone (right image) showing nuclear signal with *lacO*/LacI foci (cyan). Propidium Iodide (PI) staining (magenta). Scale bar, 10µm. (**c**) MSD analysis of *lacO*/LacI lines based on time-lapse experiments of nuclei in the division (n=116 nuclei) and differentiated zone (n=21 nuclei). 3D stacks were taken at 6sec intervals for 5min. The radius of constraint was calculated from MSD curves. Values represent means ± SEM. Student t-test, ***P < 0.001. (**d**) Left: Representative images of atrichoblast (A) and trichoblast (T) in the division zone showing nuclear signal with *lacO*/LacI foci (cyan). Propidium Iodide (PI) staining (magenta). Scale bar, 10µm. Right: Histogram of nuclear areas (µm2) from atrichoblast and trichoblast cells. Atrichoblast (n = 53 nuclei); red, Trichoblast (n = 57 nuclei); orange. (**e**) Left: MSD analysis of *lacO*/LacI lines based on time-lapse experiments of nuclei in the atrichoblast (n=36 nuclei) and trichoblast (n=61 nuclei). Right: Radius of constraint calculated from MSD curves. Values represent means ± SEM. Student t-test, ***P < 0.001.

cells from the division zone (Fig. 1C). These results confirmed that our method is suitable to unpick differences in chromatin mobility between cells. In Arabidopsis root, differences in nucleus size are often evident, not only between nuclei from the division and differentiated zones but also within the meristem itself. As such, we thought to verify if our MSD measurements would be affected by differences in nucleus size. Within the meristematic region from the root, cells have the same ploidy level (diploid), but nuclei of atrichoblast cells are considerably bigger than that of trichoblast cells (Fig. 1D). Nevertheless, these two cell types show the same chromatin mobility and radius of constraint

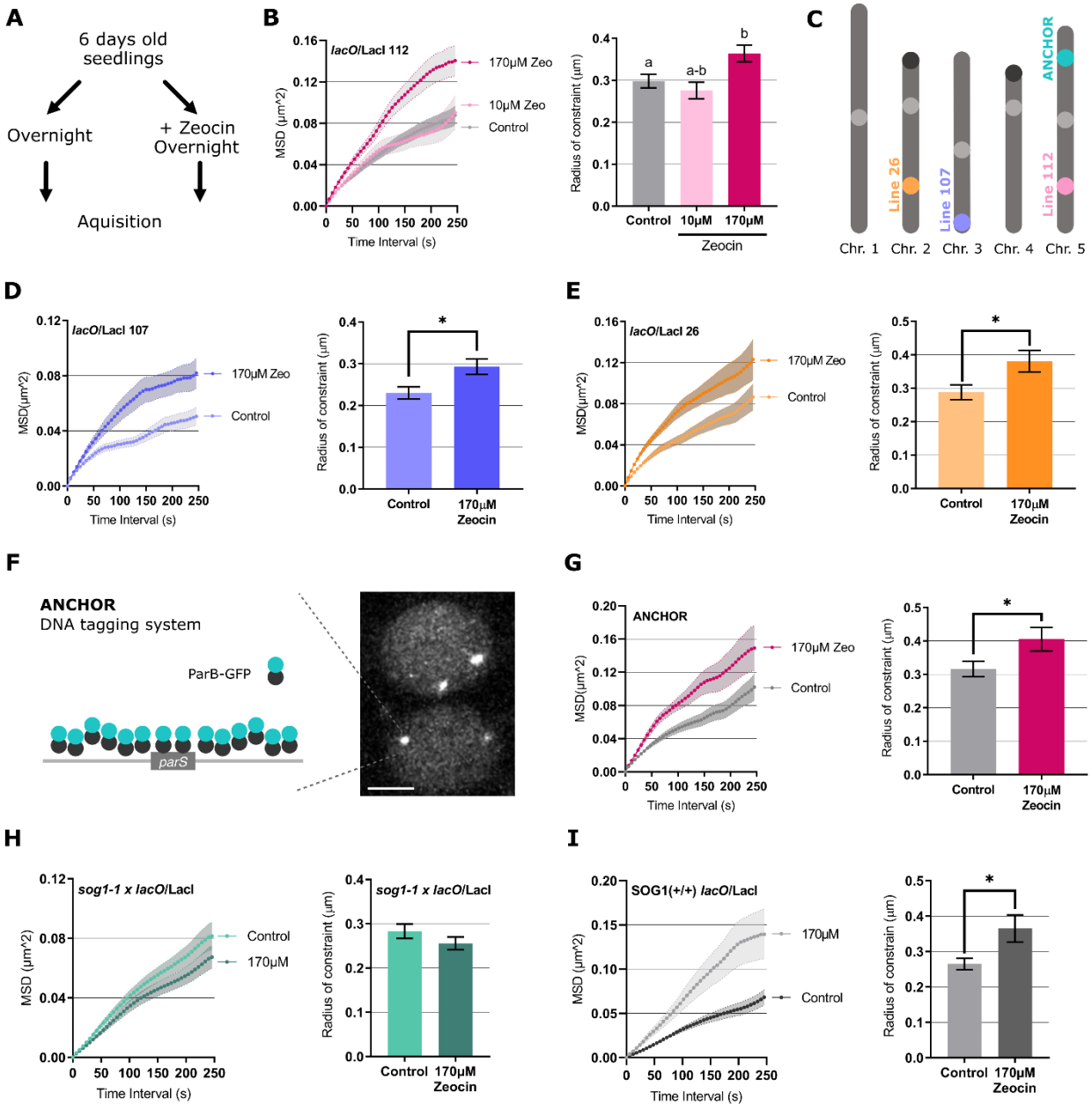

Figure 2: Chromatin mobility increases upon high DNA damage levels. (**a**) Scheme illustrating the experimental setup. (**b**) MSD analysis of *lacO*/LacI line 112 based on time-lapse experiments of nuclei in different zeocin concentrations. 10µM (n=97 nuclei); 170µM (n=93 nuclei). Radius of constraint were calculated from MSD curves. Values represent means ± SEM. Letters indicate one-way ANOVA; Bonferroni's test ($p < 0.05$).. (**c**) Chromosomal positions of *lacO*/LacI lines as reported previously[9,10]. Line 26 and line 107 are respectively inserted in chromosomes 2 and 4. The ANCHOR construct is inserted in chromosome 5. The NORs are marked as black circles and the centromeres as ligh grey circles. (**d**) MSD analysis of *lacO*/LacI line 107 based on time-lapse experiments of nuclei in control conditions and zeocin treated plants with170µM. Control (n=53 nuclei), 170µM (n=48 nuclei). Bottom: Radius of constraint calculated from MSD curves. Student t-test, *P < 0.05. **(e)** MSD analysis of *lacO*/LacI line 26 based on time-lapse experiments of nuclei upon zeocin. Control (n=52 nuclei), 170µM (n=52 nuclei). Radius of constraint calculated from MSD curves. Student t-test, *P < 0.05. (**f**) Left: Schematic representation of the ANCHOR system. *parS*-ParB:GFP interactions and oligomerization along the flanking genomic region. ParB-GFP can directly bind to parS sequence as a dimer and along the flanking genomic region. Right: Representative image of epidermis nuclei in the division zone. Scale bar, 5µm. (**g**) MSD analysis of ANCHOR line based on time-lapse experiments of nuclei upon zeocin treatment. Control (n=54 nuclei), 170µM (n=22 nuclei). Radii of constraint calculated from MSD curves. Student t-test, *P < 0.05. (**h**) MSD analysis of *lacO*/LacI line 112 crossed with *sog1-1* (Control (n=83 nuclei); 170µM zeocin (n=91 nuclei)); (**i**) MSD analysis of SOG1+/+ *lacO*/LacI progeny from crossing with *sog1-1* (Control (n=59 nuclei); 170µM zeocin (n=29 nuclei)). Radius of constraint calculated from MSD curves. Student t-test, *P < 0.05. For all MSD curves, values represent means ± SEM.

(Fig. 1E), ruling out that the nuclear volume *per se* could affect overall chromatin mobility levels.

Because HR requires pairing of the broken DNA molecule with a homologous undamaged template, we tested whether Arabidopsis cells actively regulate the chromatin mobility in response to DSBs to promote conservative repair mechanisms. We induced DNA damage by incubating 6d-old seedlings with the DSB inducer zeocin for 24h (Fig. 2A). This treatment led to the upregulation of the DDR responsive genes PARP2, RAD51 and BRCA1, indicating that the HR was effectively stimulated (Supplementary Fig. 1A). Single-molecule RNA FISH (smFISH) confirmed that the upregulation of RAD51 upon zeocin treatment is dose-dependent, with more cells responding and more transcripts per cell with increasing zeocin concentrations (Supplementary Fig.1B-C). This provided us with a system to induce different levels of DNA damage and repair mechanisms. We further focused our analysis on cells within the division zone since previous studies showed that the principal actors of HR, RAD51 and RAD54 are mainly expressed in these cells within the root [15,16]. MSD analysis revealed that *lacO*/LacI foci mobility was not changed upon low concentrations or shorter times of zeocin incubation but increased significantly with high concentrations of zeocin for 24h (Fig. 2B, Supplementary Fig. 2A B). Importantly, the effect seen at the higher concentration was not due to DNA damage-induced programmed cell death as tested by PI staining (Supplementary Fig. 3). Only stem cells and their early descendants, which are known to be highly sensitive to DNA damage[17], showed PI-positive cells but not the epidermal cells used in our chromatin mobility analysis. In order to test if the observed chromatin mobility changes were specific to zeocin treatment, we tested another DSB inducer chemical - mitomycin C (MMC). A similar increase in chromatin mobility was observed in response to MMC treatment (Supplementary Fig. 4). We also tested whether the increase in mobility upon zeocin treatment was specific for that particular *lacO*/LacI line (line112, with insertion on chr 5). To address this question, we analyzed additional *lacO*/LacI lines with insertions at different chromosomal locations (Fig. 2C). In control conditions, line 26 shows the same chromatin mobility as line 112, whereas line 107 showed significantly lower chromatin mobility and Rc (Supplementary Fig. 5). The lower mobility in line 107 could be linked to the transgene insertion at the subtelomeric region[18–20] (Fig. 2C). Upon treatment with high zeocin concentration, all lines showed a significant increase in chromatin mobility and Rc (Fig. 2D and E), further indicating that chromatin mobility increases globally in the nucleus in response to DNA damage. We also tested whether these results could be an artefact of the *lacO*/LacI system itself. For that, we performed the same experiments using another locus tagging system - the ANCHOR system (ParB-*parS*). The ANCHOR system is composed of a DNA target sequence (*parS*) 1 kb long that specifically binds ParB proteins and spread on the neighbouring region to form a larger tagged sequence[21] (Fig. 2F). The ANCHOR line showed a similar increase in chromatin mobility, suggesting that these mobility changes are a general response to DNA damage (Fig. 2G). To determine whether the increase in DNA mobility was part of the DNA damage response, we quantified *lacO*/LacI (line 112) mobility in *sog1-1* mutant, in which DDR is abolished. MSD analysis in *sog1-1* mutant revealed no increase in mobility upon treatment with high zeocin concentration, indicating that the increase of mobility seen in WT (SOG1+/+ progeny from the F1) was dependent on *SOG1* and thus on DDR activation (Fig. 2H and I). We conclude that the increase in chromatin mobility induced by zeocin treatment is actively regulated in response to DNA damage and not a physical by-product from extensive DNA “fragmentation”.

Upon DNA damage, SOG1 controls the expression of genes involved in DNA repair but also genes regulating cell cycle progression, such as CYCB1-1, leading to cell cycle arrest[23]. Since DNA content and cohesion differ in different cell cycle phases, we sought to test if changes in cell cycle dynamics (i.e. the proportion of cells in different cell cycle phases) could explain the increased chromatin mobility observed in response to DNA damage. To test this hypothesis, we crossed the *lacO*/LacI (line 112) with the S/G2 reporter CDT1a::RFP[24] (Fig. 3A, B). To first verify that this setup was working as expected, we quantified the ratio of cells in S/G2 in root epidermal cells treated with Hydroxyrea (HU), a drug blocking cells in S phase[25,26]. Indeed, we observed that there was a higher proportion of cells in S/G2 in HU samples, confirming our ability to visualize cells in S/G2 within this line (Fig. 3C). Consistently with previous studies[27], treatment with 10μM zeocin significantly increased the number of

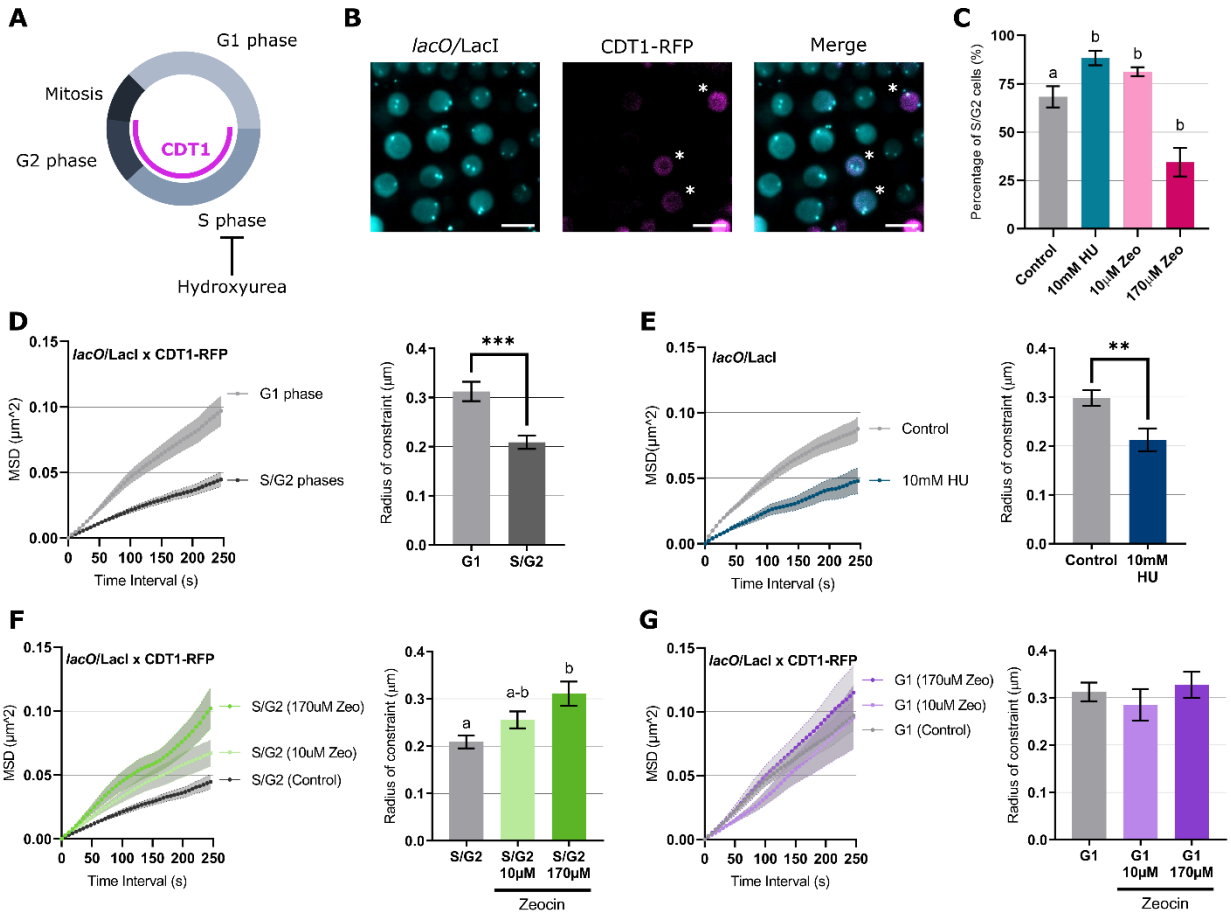

Figure 3: Chromatin mobility increases specifically during in S/G2 phases in response to DNA damage. (**a**) Schematic representation of cell cycle progression with the CDT1-RFP signal displayed in cell in S/G2. (**b**) Representative images of nuclei from *lacO*/LacI line 112 crossed with CDT1-RFP, *lacO*/LacI (cyan) CDT1-RFP (magenta) . Stars represent cells in S-G2. Scale bar, 10μm. (**c**) Percentage of S/G2 cells per root in control conditions and upon 10μM hydroxyurea, 10μM and 170μM Zeocin. (**d-h**) MSD curves and corresponding Rc histograms for: (**d**) MSD measurements of nuclei in G1 (n=62 nuclei) and S/G2 phase (n=67 nuclei); (**e**) *lacO*/LacI lines based on time lapse experiments of nuclei upon 10μM HU treatment phase (n=28 nuclei); (**f**) S/G2 cells upon different zeocin concentration (10μM (n=60 nuclei); 170μM (n=49 nuclei)); (**g**) G1 cells upon different zeocin concentration (10μM (n=35 nuclei); 170μM (n=50 nuclei)); Values represent means ± SEM. Student t-test, *P < 0.05 **P < 0.01 ***P < 0.001. Letters indicate one-way ANOVA; Bonferroni's test ($p < 0.05$)

cells in G2/S (Fig. 3C). However, with the highest concentration of zeocin (170μM), the ratio of cells in S/G2 phase decreased to half in comparison with control conditions (Fig. 3C), suggesting an accumulation of cells in G1. Therefore, we tested if G1 cells had different chromatin mobility compared to S/G2 cells. MSD analysis revealed that cells in the S/G2 phase (CDT1a-RFP positive cells) showed lower chromatin mobility than G1 cells (Fig. 3D). Similarly, HU-treated cells, showed lower chromatin mobility, most likely due to cells being arrested in the S/G2 phase (Fig. 3E). These results revealed that an accumulation of cells in G1, could explain the increased mobility. If this is the case, we hypothesized that zeocin should not increase mobility when comparing cells at the same stage of the cell cycle. We, therefore, measured the chromatin mobility specifically at G1 and S/G2, in control conditions and upon treatment with different concentrations of zeocin. We observed a significant increase in chromatin mobility in cells at S/G2 after zeocin treatment, whereas cells in G1 did not show any significant change (Fig. 3F and G). We, therefore, concluded that the increased mobility observed in response to DNA damage at high zeocin concentrations (170μM) could be both a result of an accumulation of cells in G1 and a

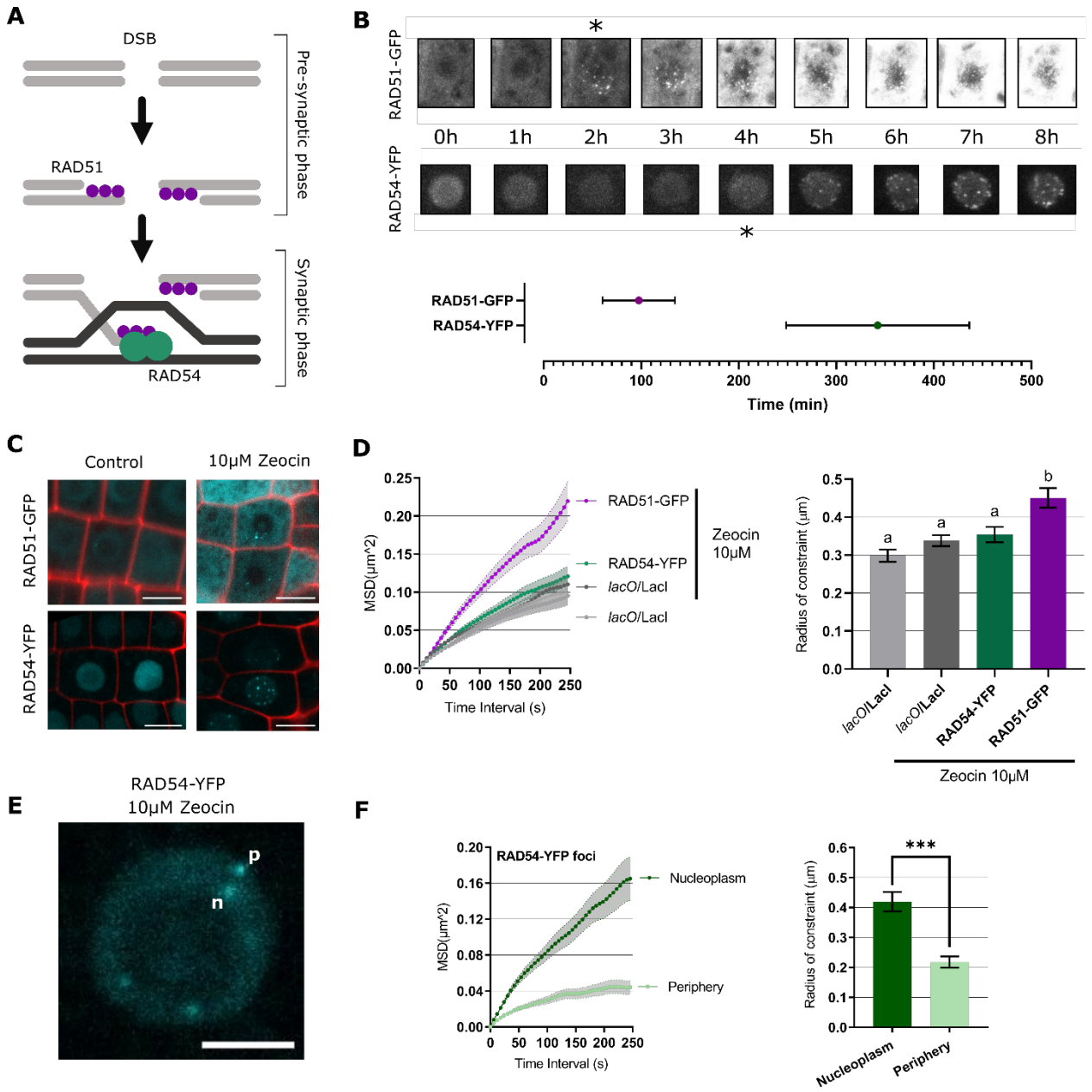

Figure 4: DSB mobility is higher at early HR. (**a**) Schematic representation of the critical steps of homologous recombination. Rad51 (purple) assemble onto the single-stranded DNA (ssDNA) formed after exonucleation of DNA double-strand break (DSB) ends to form a filament, which is known as the presynaptic filament. After searching for DNA homologous sequence, the presynaptic filament binds the DNA template to form the synaptic structure with RAD54. The ssDNA invades the homologous region in the duplex to form a DNA joint, known as the displacement (D)-loop promoted by Rad54 (green). (**b**) Time-lapse experiment of the formation of RAD51-GFP and RAD54-YFP foci in Arabidopsis nuclei, which was imaged every 30min after zeocin treatment. Timeline of RAD51 and RAD54 foci formation for 8h. Error bars indicate the standard error. At least four roots were counted for each group. (**c**) Representative images of root epidermal cells showing foci formation in RAD51-GFP and RAD54-YFP plants after 10µM zeocin treatment for 48h. Propidium Iodide (PI) staining (red). Scale bar, 10µm. (**d**) MSD analysis of RAD51 (n=64 nuclei) and RAD54 (n=64 nuclei) foci and *lacO*/LacI (line112) (n=109 nuclei) plants upon 10µM zeocin. Radius of constraint calculated from MSD curves. (**e**) Representative images of root epidermal nuclei with RAD54 foci located on the nuclear periphery (p) and in the nucleoplasm (n). Scale bar, 5µm (**f**) MSD analysis of RAD54 foci in the periphery (n=24 nuclei) and nucleoplasm (n=30 nuclei) upon 10µM zeocin. Radius of constraint calculated from MSD curves. Values represent means ± SEM. Student t-test, ***P < 0.001. Letters indicate one-way ANOVA; Bonferroni's test ($p < 0.05$)

specific increase in chromatin mobility at S/G2 phase. This observation is consistent with the idea that HR may be particularly relevant in G2 when sister chromatids have been synthesized and suggests that DDR actively increases DNA mobility in response to DSBs to promote physical search during homology-directed DNA repair.

In yeast, as in plants, studies have shown that HR is executed mainly during S/G2 phases of the cell cycle[23,28]. Because the increase in mobility upon zeocin treatment was specific to S/G2, we sought to investigate the mobility of DSBs during HR. Homologous recombination is divided into two main phases: the presynaptic phase, which includes 5'-end resection and homology search, and the synaptic phase, which includes the strand invasion for homologous strand pairing (Fig. 4A)[29]. The two main actors of HR, RAD51 and RAD54, function respectively in the initiation of the strand invasion and at the strand exchange reaction that finalizes the repair[30]. We wanted to investigate how the increase in chromatin mobility is placed in relation to these two phases. By performing an eight-hour time course experiment on RAD51-GFP and RAD54-YFP lines after induction of damage with 10μM zeocin, we were able to visualize the appearance of foci with accumulations of these proteins in the nucleus. This experiment revealed that RAD51-GFP foci were formed approximately 1h30min after DSB induction, whereas RAD54-YFP foci appeared later, at around 5h after treatment (Fig. 4B). We also observed that RAD51-GFP signal increased continuously throughout the time course experiment. This continuous raise in fluorescence signal can be explained by the C-terminus tagging of RAD51, which impairs strand exchange during the synaptic phase[15,31]. From this experiment, we could confirm that RAD51 interacts first with DSBs, while RAD54 comes in later. To investigate the mobility of foci tagged with these proteins, we treated RAD51-GFP and RAD54-YFP plants with 10μM zeocin, (Fig. 4C). The MSD analysis revealed that only RAD51 showed significantly higher mobility than *lacO*/LacI foci (Fig.4D), showing that high mobility levels seem to be associated with early HR. In Arabidopsis, as in yeast, studies have shown that RAD54 foci relocate to the nuclear periphery after γ-irradiation[32,33]. Therefore, our MSD results for RAD54 may correspond to a mixture of foci located at the nuclear periphery and at the nucleoplasm. To test if RAD54 at the different nuclear compartments behaved differently, we determined the MSD for RAD54 foci at these two nuclear locations (Fig.4E). The results showed that nucleoplasmic RAD54 foci have much higher mobility than the foci at the periphery (Fig.4F), revealing that RAD54 foci can, depending on their location, have mobilities similar to those of RAD51. Moreover, these results highlighted that large changes in chromatin mobility occur during the repair process – a strong increase in DSB mobility is observed in the early HR phase, with a subsequent drastic drop in mobility associated with the relocation of DSBs to the nuclear periphery. This relocation to the nucleus periphery has been associated with different possible roles - to bring homologous sequences together, thereby reducing the 3D search to a 2D scale [32]; or due to the fact that the repair machinery may specifically interact with nucleopores [33].

Our analysis of chromatin movement in plant living cells has revealed that an increase in chromatin mobility occurs in response to DSBs. This increase in mobility is specific for cells in S/G2 phase of the cell cycle and dependent on the DDR master regulator SOG1. These results point towards a general mechanism of response to DNA damage across kingdoms[34–37]. Additionally, DSB site mobility measured by RAD51-GFP reporter showed particularly high mobility levels compared to "steady-state" chromatin mobility and global chromosome mobility in response to DNA damage. Our results support the notion that DSBs modify chromatin mobility both locally and globally. These changes could act as a mechanism that facilitates homology search by assisting DSBs in efficiently scanning larger nuclear spaces to locate a homologous template for repair.

MATERIAL AND METHODS

Plant lines and growth conditions

Mutants and transgenic lines used in this study come from the following sources: *sog1-1*[2], RAD51-GFP[15], RAD54-eYFP[38], Cytrap line[24], *lacO*/LacI lines[9], ANCHOR line[21]. All mutants and transgenic lines are in Columbia background.

To visualize S/G2 cells, *lacO*/LacI line 112 was crossed to Cytrap line, and the resulting F_2 plants were selected on MS plates containing 50 mg/L of kanamycin (Sigma-Aldrich, catalogue number K1377). Because the G2/M-marker CYCB1;1 is strongly expressed during DNA damage[39], the selected F_2 were screened only for LacI-GFP and CDT1a-RFP.

Seeds were sterilized in 5% v/v sodium hypochlorite for 5 min and rinsed three times in sterile distilled water. Seeds were stratified at 4°C for 48 h in the darkness. Seeds were then plated on Murashige and Skoog (MS) medium and then grown in 16 hours light at 25°C in vertically oriented Petri dishes. The roots were observed after 6 to 7d of incubation, depending on the experiment.

Genotoxic treatment

To induce DNA damage response, 5- to 6-day-old seedlings were transferred in MS medium without or with 100 µM mitomycin C (MMC); 2, 10, 50, 100 or 170 µM zeocin or 10 mM hydroxyurea (HU) and treated for 2h, 6h, or 24h. Each chemical was obtained respectively from Fisher Scientific (catalogue number 2980501), Invitrogen (catalogue number R25001) and Sigma-Aldrich (catalogue number H8627-1G).

smFISH on root squashes

smFISH was carried out as described by Duncan et al. 2016. Briefly, root tips from 7-day-old seedlings were cut using a razor blade and placed into glass wells containing 4% paraformaldehyde and fixed for 30 min. Roots were then removed from the fixative and washed twice with nuclease-free 1X PBS. Several roots were then arranged on a microscope slide and squashed between the slide and coverslip. Slides were submerged (together with the coverslips) for a few seconds in liquid nitrogen until frozen. The coverslips were then removed, and the roots were left to dry at room temperature for 30 min.

Tissue permeabilization and clearing were achieved by immersing the samples sequentially in 100% methanol for one h, 100% ethanol for 1h and 70% ethanol for a minimum of one hour. The ethanol was left to evaporate at room temperature for 5 min, and slides were then washed with Stellaris RNA FISH Wash Buffer A (Biosearch Technologies Cat# SMF-WA1-60). 100µl of hybridization solution (containing 10% dextran sulfate, 2x SSC and 10% formamide), with each probe set at a final concentration of 125nM, was then added to each slide. The slides were left to hybridize at 37°C overnight in the dark.

The hybridization solution containing unbound probes was pipetted out the following morning. Each sample was then washed twice with Stellaris RNA FISH Wash Buffer B (Biosearch Technologies Cat# SMF-WB1-20) with the second wash left to incubate for 30 min at 37°C. 100µl of the nuclear stain DAPI (100ng/mL) was added to each slide and left to incubate at 37°C for 10 minutes. Slides were then quickly washed with 2xSSC. 100µl GLOX buffer minus enzymes (0.4% glucose in 10mM Tris, 2X SSC) was added to the slides and left to equilibrate for 2 min. Finally, 100µl of GLOX buffer containing the enzymes glucose oxidase and catalase, where 1µl of each enzyme (Glucose oxidase (#G0543 from Sigma) and catalase (#C3155 from Sigma) was added to a total of 100µl of GLOX minus enzymes. The samples were then covered by 22mm x 22mm No.1,5 coverslips (VWR), sealed with nail varnish and immediately imaged.

We used the online program Stellaris Probe Designer version 2.0 from Biosearch Technologies to design probe sequences for RAD51 mRNA and unspliced transcripts. For probe sequences, see Supplementary Table 1.

Microscopy

For root staining with propidium iodide (PI) 6 to 7-d-old seedlings were mounted in water between slide and coverslip and sealed with 0.12-mm-thick SecureSeal Adhesive tape (Grace Bio-Labs) to reduce drift drying during imaging.

For smFISH, samples were imaged using a Zeiss LSM800 inverted microscope, with a 63x water-immersion objective (1.20 NA) and Microscopy Camera Axiocam 503 mono; Quasar570 were detected using a 533-558nm excitation filter by collecting the signal between 570-640 nm. For DAPI, an excitation filter 335-383nm was used, and the signal was detected between 420-470 nm

Mean square displacement

For all MSD experiments, time-lapse imaging was performed every 6 s, taking a Z-stack of 3 µm spread through 1µm slices for 5 min, with a 512 × 512 pixels format with a 1-2× zoom factor. All images were analyzed using Fiji software (NIH, Bethesda, MD, http://rsb.info.nih.gov/ij/) (Sage et al. 2005) and with the plugin SpotTracker 2D (obtained from http://bigwww.epfl .ch/sage/soft/spottracker). Images were analyzed as described in Meschichi *et al.* ,2021.

Expression Analysis Using Real-Time RT-PCR (qPCR)

Seedlings grown for 7 d were harvested, and total RNA was extracted using the Trizol reagent (Invitrogen). A total of 1 µg of RNA was treated with TURBO DNase (Life Technologies) and used for cDNA synthesis (Superscript IV; Life Technologies). The resulting cDNA was diluted 10 times and used for quantitative PCR using a Bio-Rad iCycler Thermal Cycler iQ5 Multicolor Real-Time and HOT FIREPol® EvaGreen® qPCR Mix Plus (Solis Biodyne). For data normalization, the data were first normalized to the PP2A2 reference gene, and the values from two independent samples were normalized to the average Delta Ct value Col-0 level or control condition (2^-ΔΔCt Method). The final values presented are given as the mean ± SD from three independent samples. Minus RT (no reverse transcriptase control) controls were set up to make sure the values reflect the level of RNA and not DNA contamination. The standard Student's t-test was used to determine the statistical significance of the results. The primers used are listed in Supplementary Tables 2.

Statistical analysis

For statistical analysis, we used the GraphPad Prism 8.3 software. Data set were tested for normality using the Shapiro–Wilk test. Statistical significance was determined by using the standard student t-test (two-tailed) and one-way ANOVA (multiple comparisons with Bonferroni correction. All experiments were performed in several nuclei as mentioned in figure legends and in Supplementary Table 3.

COMPETING INTEREST STATEMENT

ANCHOR system is the property of NeoVirTech SAS, Toulouse, France. Any request of use should be addressed to contact@neovirtech.com.

ACKNOWLEDGMENTS

We thank Susan Gasser and Anais Cheblal for the SpotTracking and Excel Macro, Charles White for RAD51-GFP line, Anne Britt for the *sog1-1* mutant, Sashihiro Matstunaga for RAD54-eYFP line, Masaaki

Umeda and Shiori Aki for the Cytrap line and Confocal Microscopy Platform from SLU, Uppsala, Sweden. We thank Marion Orsucci for help with the statistical analysis. We thank Lauriane Simon for comments on the manuscript. This work was supported by the Swedish Research Council (Vetenskapsrådet) grant number 2018-04101. We would like to thank COST ACTION CA16212 INDEPTH for the inputs and comments.

AUTHOR CONTRIBUTION

AM, SR, FP and AS designed the experiments. AM and SvR performed the experiments. AM, SR, FP and AS analyzed the data. All authors contributed to writing the article and approved the submitted version.

REFERENCES

1. van Gent, D. C., Hoeijmakers, J. H. J. & Kanaar, R. Chromosomal stability and the DNA double-stranded break connection. *Nat. Rev. Genet.* **2**, 196–206 (2001).

2. Yoshiyama, K., Conklin, P. A., Huefner, N. D. & Britt, A. B. Suppressor of gamma response 1 (SOG1) encodes a putative transcription factor governing multiple responses to DNA damage. *Proc. Natl. Acad. Sci.* (2009). doi:10.1073/pnas.0810304106

3. Yoshiyama, K. O. *et al.* ATM-mediated phosphorylation of SOG1 is essential for the DNA damage response in Arabidopsis. *EMBO Rep.* (2013). doi:10.1038/embor.2013.112

4. Bourbousse, C., Vegesna, N. & Law, J. A. SOG1 activator and MYB3R repressors regulate a complex DNA damage network in Arabidopsis. *Proc. Natl. Acad. Sci.* **115**, E12453–E12462 (2018).

5. Jackson, S. P. Sensing and repairing DNA double-strand breaks. *Carcinogenesis* **23**, 687–696 (2002).

6. West, C. E., Waterworth, W. M., Sunderland, P. a & Bray, C. M. Arabidopsis DNA double-strand break repair pathways. *Biochem. Soc. Trans.* **32**, 964–6 (2004).

7. Nisa, M.-U., Huang, Y., Benhamed, M. & Raynaud, C. The Plant DNA Damage Response: Signaling Pathways Leading to Growth Inhibition and Putative Role in Response to Stress Conditions. *Front. Plant Sci.* **10**, (2019).

8. Puchta, H. The repair of double-strand breaks in plants: mechanisms and consequences for genome evolution. *J. Exp. Bot.* (2004). doi:10.1093/jxb/eri025

9. Matzke, A. J. M., Watanabe, K., van der Winden, J., Naumann, U. & Matzke, M. High frequency, cell type-specific visualization of fluorescent-tagged genomic sites in interphase and mitotic cells of living Arabidopsis plants. *Plant Methods* (2010). doi:10.1186/1746-4811-6-2

10. Matzke, A. J. M., Lin, W. & Matzke, M. Evidence That Ion-Based Signaling Initiating at the Cell Surface Can Potentially Influence Chromatin Dynamics and Chromatin-Bound Proteins in the Nucleus. **10**, 1–16 (2019).

11. Horigome, C., Dion, V., Seeber, A., Gehlen, L. R. & Gasser, S. M. Visualizing the Spatiotemporal Dynamics of DNA Damage in Budding Yeast. *Methods Protoc.* **1292**, 77 (2015).

12. Meschichi, A. & Rosa, S. Visualizing and Measuring Single Locus Dynamics in Arabidopsis thaliana. in *Arabidopsis Protocols* (eds. Sanchez-Serrano, J. J. & Salinas, J.) 213–224 (Springer US, 2021). doi:10.1007/978-1-0716-0880-7_10

13. Rosa, S. *et al.* Cell Differentiation and Development in Arabidopsis Are Associated with Changes in Histone Dynamics at the Single-Cell Level. *Plant Cell* **26**, 1–14 (2014).

14. Arai, R. *et al.* Reduction in chromosome mobility accompanies nuclear organization during early embryogenesis in Caenorhabditis elegans. *Sci. Rep.* **7**, 3631 (2017).

15. Da Ines, O. *et al.* Meiotic Recombination in Arabidopsis Is Catalyzed by DMC1, with RAD51 Playing a Supporting Role. *PLoS Genet.* (2013). doi:10.1371/journal.pgen.1003787

16. Hirakawa, T., Hasegawa, J., White, C. I. & Matsunaga, S. RAD54 forms DNA repair foci in response to DNA damage in living plant cells. *Plant J.* **90**, 372–382 (2017).

17. Fulcher, N. & Sablowski, R. Hypersensitivity to DNA damage in plant stem cell niches. *Proc. Natl. Acad. Sci.* **106**, 20984–20988 (2009).

18. Armstrong, S. J., Franklin, F. C. & Jones, G. H. Nucleolus-associated telomere clustering and pairing precede meiotic chromosome synapsis in Arabidopsis thaliana. *J. Cell Sci.* **114**, 4207–17 (2001).

19. Fransz, P., de Jong, J. H., Lysak, M., Castiglione, M. R. & Schubert, I. Interphase chromosomes in Arabidopsis are organized as well defined chromocenters from which euchromatin loops emanate. *Proc. Natl. Acad. Sci.* **99**, 14584–14589 (2002).

20. Pontvianne, F. *et al.* Identification of Nucleolus-Associated Chromatin Domains Reveals a Role for the Nucleolus in 3D Organization of the A. thaliana Genome. *Cell Rep.* **16**, 1574–1587 (2016).

21. Meschichi, A. *et al.* ANCHOR: A Technical Approach to Monitor Single-Copy Locus Localization in Planta. *Front. Plant Sci.* **12**, (2021).

22. Furukawa, T. *et al.* A shared DNA-damage-response pathway for induction of stem-cell death by UVB and by gamma irradiation. *DNA Repair (Amst).* **9**, 940–948 (2010).

23. Weimer, A. K. *et al.* The plant-specific CDKB1-CYCB1 complex mediates homologous recombination repair in Arabidopsis. *EMBO J.* **35**, 2068–2086 (2016).

24. Yin, K. *et al.* A dual-color marker system for in vivo visualization of cell cycle progression in Arabidopsis. *Plant J.* **80**, 541–552 (2014).

25. Singh, A. & Xu, Y.-J. The Cell Killing Mechanisms of Hydroxyurea. *Genes (Basel).* **7**, 99 (2016).

26. Cools, T., Iantcheva, A., Maes, S., Van den Daele, H. & De Veylder, L. A replication stress-induced synchronization method for Arabidopsis thaliana root meristems. *Plant J.* **64**, 705–714 (2010).

27. Chen, P. *et al.* Arabidopsis R1R2R3-Myb proteins are essential for inhibiting cell division in response to DNA damage. *Nat. Commun.* **8**, 635 (2017).

28. Ferreira, M. G. Two modes of DNA double-strand break repair are reciprocally regulated through the fission yeast cell cycle. *Genes Dev.* **18**, 2249–2254 (2004).

29. Wright, W. D., Shah, S. S. & Heyer, W.-D. Homologous recombination and the repair of DNA double-strand breaks. *J. Biol. Chem.* **293**, 10524–10535 (2018).

30. Solinger, J. A. & Heyer, W.-D. Rad54 protein stimulates the postsynaptic phase of Rad51 protein-mediated DNA strand exchange. *Proc. Natl. Acad. Sci.* **98**, 8447–8453 (2001).

31. Kobayashi, W., Sekine, S., Machida, S. & Kurumizaka, H. Green fluorescent protein fused to the C terminus of RAD51 specifically interferes with secondary DNA binding by the RAD51-ssDNA complex. *Genes Genet. Syst.* **89**, 169–179 (2014).

32. Seeber, A. & Gasser, S. M. Chromatin organization and dynamics in double-strand break repair. *Curr. Opin. Genet. Dev.* **43**, 9–16 (2017).

33. Nagai, S. *et al.* Functional Targeting of DNA Damage to a Nuclear Pore-Associated SUMO-Dependent Ubiquitin Ligase. *Science (80-.).* **322**, 597–602 (2008).

34. Dion, V., Kalck, V., Horigome, C., Towbin, B. D. & Gasser, S. M. Increased mobility of double-strand breaks requires Mec1, Rad9 and the homologous recombination machinery. *Nat. Cell Biol.* (2012). doi:10.1038/ncb2465

35. Dimitrova, N., Chen, Y.-C. M., Spector, D. L. & de Lange, T. 53BP1 promotes non-homologous end joining of telomeres by increasing chromatin mobility. *Nature* **456**, 524–528 (2008).

36. Miné-Hattab, J. & Rothstein, R. Increased chromosome mobility facilitates homology search during recombination. *Nat. Cell Biol.* **14**, 510–517 (2012).

37. Krawczyk, P. M. *et al.* Chromatin mobility is increased at sites of DNA double-strand breaks. *J. Cell Sci.* **125**, 2127–2133 (2012).

38. Hirakawa, T. & Matsunaga, S. Characterization of DNA Repair Foci in Root Cells of Arabidopsis in Response to DNA Damage. *Front. Plant Sci.* **10**, (2019).

39. Culligan, K. M., Robertson, C. E., Foreman, J., Doerner, P. & Britt, A. B. ATR and ATM play both distinct and additive roles in response to ionizing radiation. *Plant J.* **48**, 947–961 (2006).